CHAPTER - 4

DETERMINATION OF OPTICAL CONSTANTS AND POLARIZABILITY STUDIES ON FERROIC TETRAMETHYLAMMONIUM TETRACHOLOROZINCATE CRYSTAL

4.1 Introduction

The discovery of ferroelectricity in tetramethylammonium tetrachlorozincate compound $[N(CH_3)_4]_2ZnC1_4$ **[128]** that crystallizes in the high symmetry phase D_{4h} leading to wide numbers of experimental investigations. Among those, most of the studies concentrated on the structural phase transformations of the material due to the interesting behaviour of commensurate-incommensurate phase transition together with the many successive phase transitions. The incommensurate phase is generally characterized by the amplitudons and phasons **[129]**. The phasons could be detected only by the neutron inelastic scattering and the Brillouin scattering **[130]** whereas the soft mode behaviour of the amplitudons could be observed by Raman scattering studies. In this context, J.Berger et.al. **[131]** estimated the photoelastic coefficients of $[N(CH_3)_4]_2ZnC1_4$ by Brillouin scattering method. E.Harajamarki et.al.**[132]** also used this method for their works on phase transitions. Some authors focused on the neutron inelastic scattering to get knowledge of the dynamic behaviour of this material **[133, 134]**. Besides, neutron diffraction study on this material was undertaken by D.Durand et.al. **[135]**. Most of the experimental researchers focused on the Raman scattering studies to analyse the successive transformations of the material in different dimensions. For instance, the incommensurate phase study with group theoretical method was thoroughly explained by M.Pal et.al. **[136]**. The

Raman spectra of the parent phase and low symmetry phases of this compound were well established by V.I.Torgasev et.al. **[137, 138]**.

Few works were found to deal with the electron paramagnetic resonance (EPR) **[139]** and proton magnetic resonance **[140, 141]** to examine the internal vibrations of this material. The heat capacities of $[N(CH_3)_4]_2ZnC1_4$ were determined by T.P.Melia et.al. **[142]** and temperature-pressure diagram was established by M.Gerard et.al. **[143]**. For the past three decades wide varieties of works had been established by various solid state researchers. However, the optical properties of this material hold little attention by several groups. T. Breczewski **[144]** reported the optical activity of the centrosymmetric incommensurate phase of $[N(CH_3)_4]_2ZnC1_4$.One of the recent article **[145]** reported the study of optical transmission and nonlinear optical property of this material. A. El-Korashy **[146]** calculated the optical band gap energy of the material in paraelectric phase. There are no extensive findings in this material on the determination of optical constants such as absorption coefficient, refractive index, dielectric constant together with the polarizabilty. Bearing this is in mind, the present work illustrate the above mentioned optical properties of $[N(CH_3)_4]_2ZnC1_4$ in detail. In addition, theoretical Penn analysis has also been made in support of the experimentally calculated polarizability values.

4.2 Materials and methods

The single crystals of $[N(CH_3)_4]_2ZnC1_4$ were grown by the slow evaporation method at room temperature under normal pressure as prescribed elsewhere **[147]**. The selected good quality crystals were subjected to various studies. The crystals were subjected to single crystal X–ray diffraction using Bruker Kappa Apex II diffractometer with 0.71073 Å wavelength of radiation and the lattice parameters

were determined. The Radiant Technology method (Tester Name: PMF0713-334) was used for hysteresis loop study. Raman spectra of powder samples were measured using a micro Raman spectrometer (Rienshaw, UK, model inVia) with 514 nm laser excitation from 1 cm^{-1} to 4000 cm^{-1}. The UV – Vis transmission and reflection spectra were recorded using Cary– 300 instrument in the range 200-1100 nm with a resolution of 1 nm in the solid state. The dielectric measurements were carried out using N4L Numetric Q PSM 1735 instrument in the frequency range 1 KHz– 10 MHz. Polished grown crystal coated with silver paste was used for the measurements capacitance.

4.3 Results and Discussion

The lattice parameters a = 8.981(8) Å , b = 12.256(6) Å and c = 15.513(7) Å and V= 1707.5(14) $Å^3$ obtained from single crystal XRD study agree well with the literature values **[136]** and confirm the orthorhombic structure of the material. The recorded Raman spectrum is given in **Fig. 4.1**. Lattice vibration is appeared at 57 cm^{-1} and the symmetric stretching vibrations of $ZnCl_4$ are emerged below 350 cm^{-1}. The C-N symmetric and asymmetric deformations modes are found at 370 and 461 cm^{-1} respectively whereas the symmetric and asymmetric stretching vibrations of C-N exhibited, peaks at 761 and 958 cm^{-1} respectively. The Raman absorption peaks at 1176, 1415 and 1457 cm^{-1} are assigned to the CH_3 rocking, symmetric and asymmetric deformations respectively. The CH_3 symmetric stretching vibrations appear at 2928, 2965 and 2980 cm^{-1} and the corresponding asymmetric stretching vibration is found at 3031 cm^{-1}.

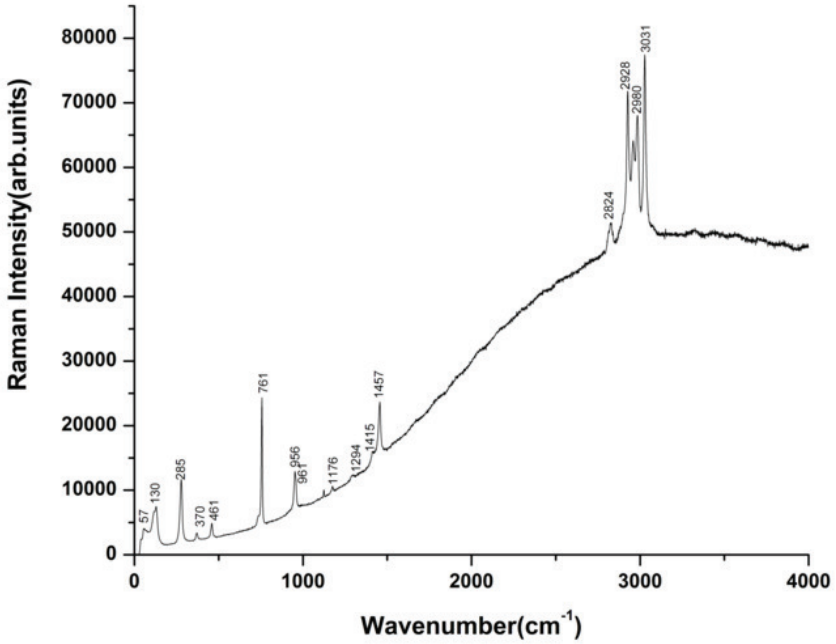

Fig. 4.1 Raman spectrum

On seeing the polarized Raman spectrum reported in the ref. **[137]** our recorded powder Raman spectrum is in good agreement with the B_{2g} vibrational modes. In general, the D_{4h} space group symmetry consists of 8 vibrational modes which are described by A_g, B_{1g}, B_{2g}, B_{3g}, A_u, B_{1u}, B_{2u} and B_{3u}. Among those, A_g, B_{1g}, B_{2g} and B_{3g} vibrational modes are Raman active while others are Infrared active. The Raman active modes are distributed as $65_{Ag}+52_{B1g}+65_{B2g}+52_{B3g}$ in the total 468 vibrational modes **[137]**. Among the 6 polarizability Raman tensor components the 3 *diagonal* tensor components belong to Ag modes and the remaining three B_{1g}, B_{2g} and B_{3g} vibrational modes correspond to the *off-diagonal* tensor components. Since the present vibrational modes belong to B_{2g} modes which has the polarizability tensor components as c(ac)a, it predict the occurrence of Raman scattering along 'a'

axis. It suggests that our grown crystal is highly oriented in the 'a' direction which referred to the shortest unit cell axes.

The ferroelectric hysteresis loop obtained (**Fig. 4.2**) using radiant technology is the evidence for the ferroelectric behaviour of the material. It is noticed that the remanant polarization increases with the applied voltages. Further, ferroelectric ceramic behaviour is identified through the resistive leakage along the grain boundaries.

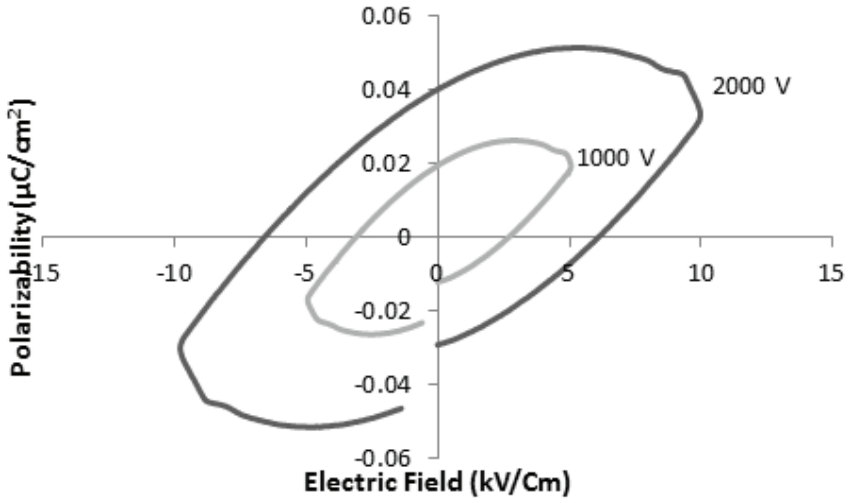

Fig. 4.2 Ferroelectric hysteresis loop study

For the determination of optical constants we have undertaken the UV-Vis transmission (T) and reflection (R) studies. The recorded transmittance spectrum displayed in **Fig. 4.3** shows a better transmittance of the material in the visible region. The absorption coefficient (α) is calculated using the recorded transmittance values as follows

$$\alpha = \frac{ln^{1}/_{T}}{t} \qquad (1)$$

where, t is the thickness of the crystal.

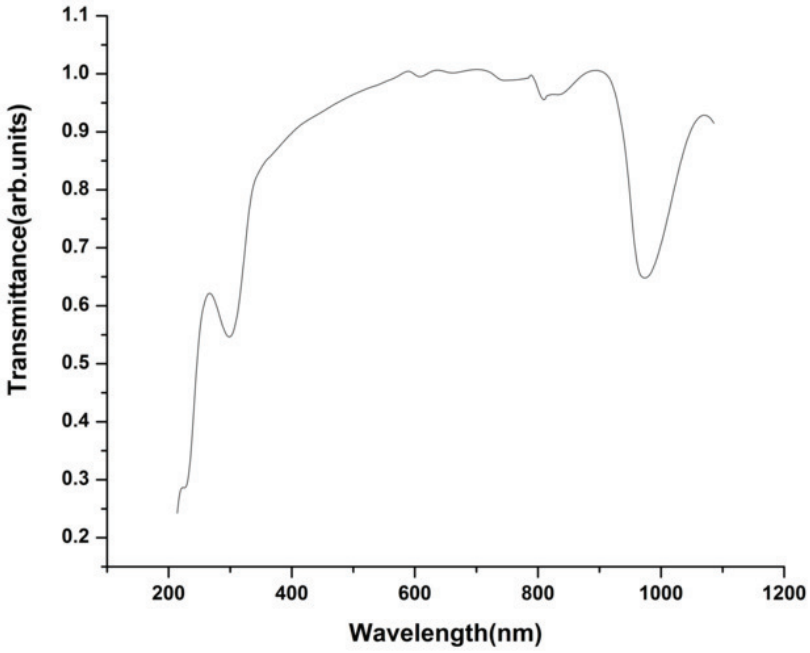

Fig. 4.3 Recorded Transmittance Spectrum

In the visible range of 575–725 nm the absorption coefficient is zero and it is very low in the other visible range 400–575 nm, predicting the insulating behaviour. The maximum absorption coefficient value obtained is of the order of 10^2 m^{-1} (**Fig. 4.4**), which exemplify the indirect optical band gap nature of the material **[147]**. The optical band gap energy is determined using the Tauc relation **[148]**:

$$\alpha h\nu = A\left(h\nu - E_g\right)^n \qquad (2)$$

where, $h\upsilon$ is the photon energy, E_g is the optical band gap, A is a constant, n = ½ for direct allowed transition and n = 2 for indirect allowed transition. In our case, n = 2 as it belongs to the indirect band gap nature of the material. Because of the lattice phonons contribution in the indirect allowed transitions the exact relationship between absorption coefficient and band gap is given by Bardeen et.al. **[149]** as:

$$\alpha h\nu = A\left(h\nu - E_g \pm E_p\right)^n \qquad (3)$$

where E_p is the lattice phonon energy .

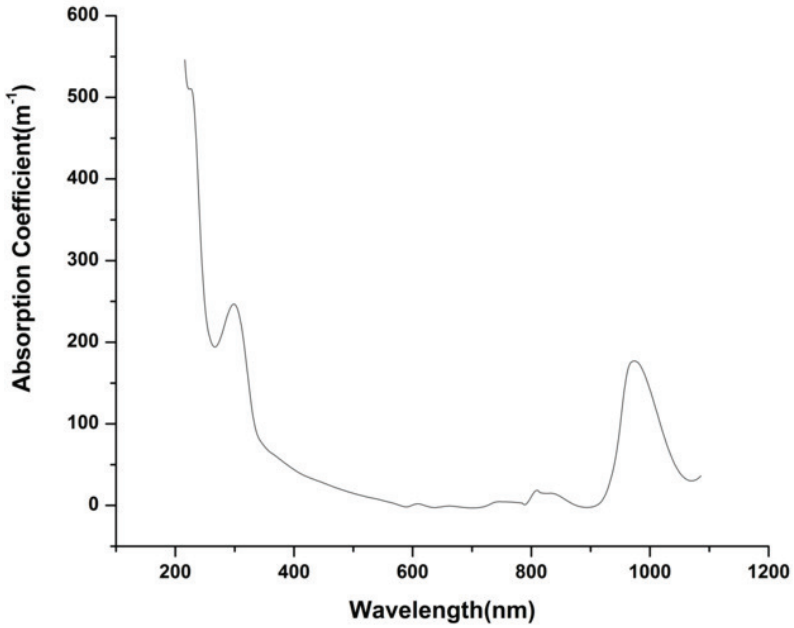

Fig. 4.4 Calculated Absorption Coefficient Spectrum

The straight line extrapolation of $(\alpha h\nu)^{1/2}$ to the zero absorption coefficient on the $x-axis$ in Tauc plot ($h\nu\ vs(\alpha h\nu)^{1/2}$) (**Fig. 4.5**) gives the optical band gap energy value. It should be noted that, there is two straight lines in Tauc plot that contribute to the two valence bands in band gap energy determination owing to the spin-orbit interaction and crystal field splitting. The intercepts of these two straight lines to zero absorption coefficient are 4.62 and 4.45 eV. Hence the exact optical bandgap energy is corrected as 4.45+0.17 eV or 4.62-0.17 eV and 0.17 eV is referred to as lattice phonon energy. The calculated indirect optical band gap energy value is in good agreement with the reported values along the 'a' axis of the crystal **[146]** and it further indicates the insulating behaviour of the material.

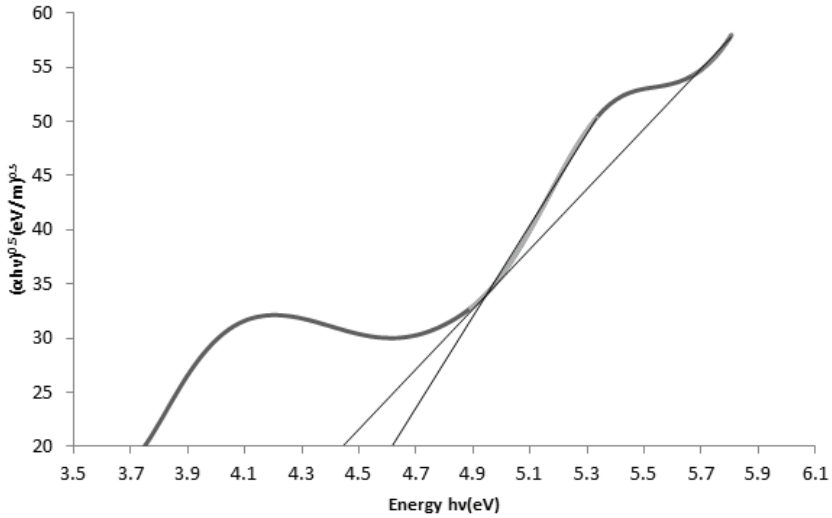

Fig. 4.5 Tauc Plot

The refractive index (n) values are calculated using the recorded reflectance (R) values by the theory of reflectivity. This theory correlates the reflectance, refractive index and extinction coefficient(k) (**Fig. 4.6**) as described by Fresnel's coefficients **[150, 151]**:

$$R = \frac{(n-1)^2 + k^2}{(n+1)^2 + k^2} \tag{4}$$

For insulating materials this equation is simplified as

$$R = \frac{(n-1)^2}{(n+1)^2} \tag{5}$$

where $k \approx 0$ (**Fig 4.6**) to satisfy $k = \alpha\lambda/4\pi$

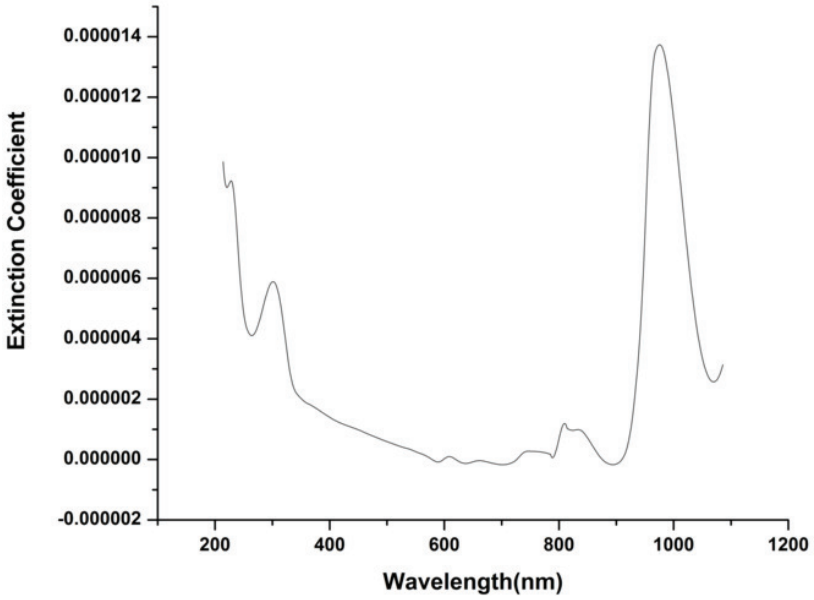

Fig. 4.6 Extinction Coefficient Spectrum

The calculated refractive index values are in the range 9.7–10.8 (**Fig. 4.7**) in the visible region (400–700 nm). On noting down the dielectric constant values there is a possibility for only the real part since $k \approx 0$. Generally the imaginary part is $\varepsilon'' = 2nk$ and the real part is $\varepsilon' = n^2 - k^2$. The calculated real dielectric constant values are very high (94.4–117.1) (**Fig. 4.8**) at the particular interest of the visible region. The large value of dielectric constants indicates the good ferroic nature of the material.

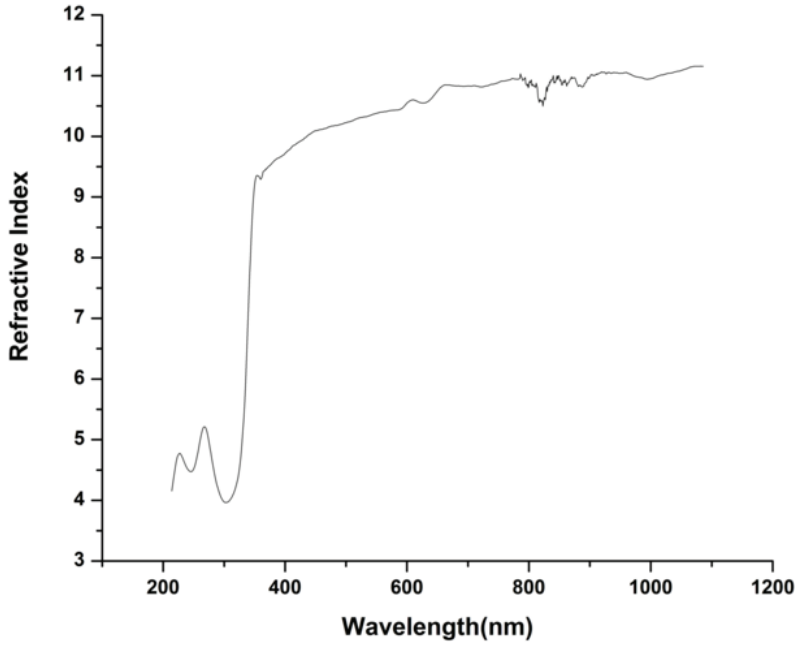

Fig. 4.7 Calculated Refractive Index Plot

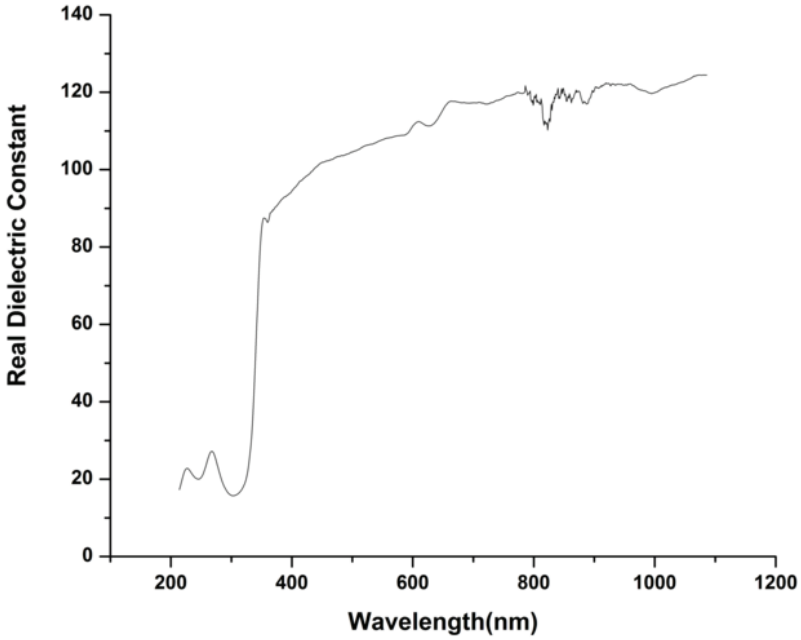

Fig. 4.8 Dielectric constant Plot

From the calculated value of dielectric constant the electronic polarizability is calculated using the Clausius-Mossotti equation **[152]** as follows

$$\alpha \simeq \left[\frac{\varepsilon_r - 1}{\varepsilon_r + 2}\right]\left[\frac{M}{\rho}\right] / 2.53 \times 10^{24} cm^3 \qquad (6)$$

where M is the molecular weight and ρ is the density of the crystal.

The calculated values of polarizability (0.844×10^{-22} – 0.992×10^{-22} cm^3) lie in the 215–1086 nm range (in terms of frequencies the range is 1.4×10^{15}-2.7×10^{14} Hz) is shown in **Fig. 4.9**. From the figure it is observed that the electronic polarizability remains constant to a certain range of increasing frequencies and then drastically decreases with further increasing of frequencies. At very high frequency regions, the polarizability increase and decrease alternately with repetition.

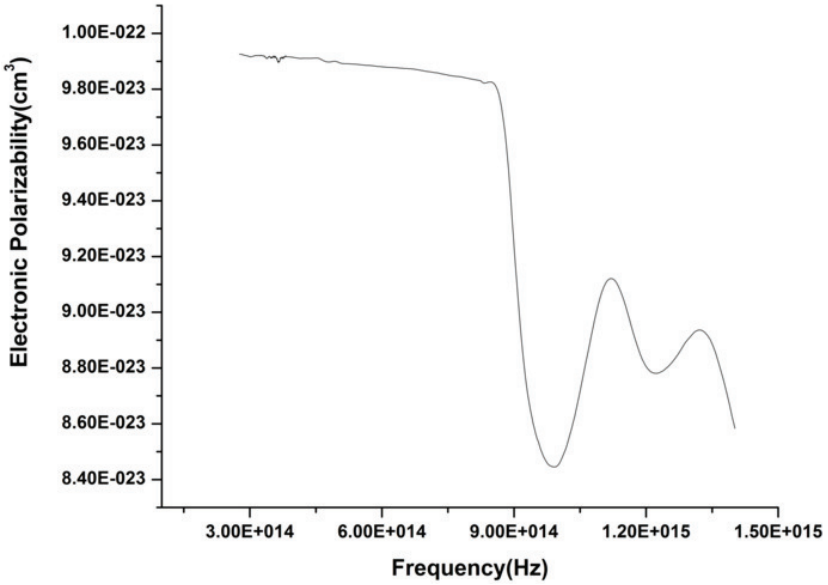

Fig. 4.9 Electronic Polarizability in the higher frequency regions

The low frequency polarizability values have been calculated through dielectric studies. The measured capacitance values of the crystal and air are used to determine the dielectric constant values of the crystal using the following equation

$$\varepsilon_r = \frac{\left[C_{cry} - C_{air}\left(\frac{1-A_{cry}}{A_{air}}\right)\right]}{C_{air}} \frac{A_{air}}{A_{cry}} \quad (7)$$

where C_{crys} is the capacitance of the crystal. C_{air} is the capacitance of air for the same dimension of the crystal, A_{crys} and A_{air} are the area of the crystal and area of the electrode respectively **[153]**. From the calculated values of dielectric constant the average polarizability has been calculated using the Clausius-Mosotti equation and it is found to be 1.007×10^{-22} cm^3.

This experimentally calculated polarizability value could be verified theoretically through Penn analysis. In general, Penn analysis **[154, 155]** focuses on the dielectric constant which depends on the Plasmon energy, Fermi energy and Penn gap along with its related properties of the wide band gap semiconductors. In our study, Penn analysis is used here as an attempt to find the polarizability value of the insulating material.

The valence electron Plasmon energy ($\hbar\omega$) is defined by as follows

$$\hbar\omega = 28.8\sqrt{\frac{Z\rho}{M}}\ (eV) \quad (8)$$

where, Z is the total number of valence states (Z = 64 for our material), ρ is the density and M is the molecular weight of the crystal.

The Fermi energy E_F is calculated as follows using $\hbar\omega$

$$E_F = 0.2947(\hbar\omega)^{\frac{4}{3}}(eV) \quad (9)$$

The polarizability value α is obtained as

$$\alpha = \left[\frac{(\hbar\omega)^2 S_0}{(\hbar\omega)^2 S_0 + 3E_p^2}\right]\frac{M}{\rho}0.396\times10^{-24}cm^3 \quad (10)$$

where E_p is the Penn gap and S_0 is a constant for the material which are defined by

$$E_p = \frac{\hbar\omega}{(\varepsilon_r - 1)^{1/2}}\ (eV) \quad (11)$$

$$S_0 = 1 - \frac{E_p}{4E_F} + \frac{1}{3}\left(\frac{E_p}{4E_F}\right)^2 \quad (12)$$

The value of the constant $S_0 = 1$ for the original Penn model, the polarizability values that correspond to S_0 nearly equal to "1" have only been considered to obtain average polarizability. The average value of S_0 is 0.991 and the calculated average polarizability value is found to be 1.009×10^{-22} cm^3 which exactly matches with the polarizability value (1.007×10^{-22} cm^3) obtained from Clausius-Mossotti equation via experimental dielectric study. In addition, the calculated Plasmon energy is found to be 14.36 eV and that of Fermi energy is 10.29 eV.

Generally, in lower frequency regions all polarizabilty components namely ionic, dipolar, space charge and electronic polarizations participate in the polarization process. In our study, the comparison between electronic polarizability in the optical region and polarizability in the lower frequency region reveals that the entire contribution of electronic polarizability is in the low frequency region. The ionic and dipolar polarization contribution are found to be least in the polarization process.

4.4 Summary and Conclusion

The ferroelectric Tetramethylammonium Tetrachlorozincate $[N(CH_3)_4]_2ZnC1_4$ crystal was synthesized by slow evaporation method. The single crystal XRD and Raman studies confirmed the formation of the material with orthorhombic structure and a high orientation of the crystal along 'a' axis. The ferroelectric behaviour was identified through ferroelectric hysteresis loop study. The calculated absorption coefficient values from the recorded transmittance values were

in the maximum order of 10^2 m^{-1} gave an indication that the material belonged to an indirect bang gap material. From Tauc plot two valence bands contribution was established in the determination of optical bandgap energy whose value is 4.45+0.17 eV or 4.62-0.17 eV for the 'a' axis orientation of this material where 0.17 eV is the lattice phonon energy. The calculated value of refractive index from the recorded reflectance values lie in the range 9.7–10.8 in the visible region and the corresponding values of real dielectric constant are in the range 94.4–117.1. The calculated electronic polarizability is in the optical frequency region covering a range 0.844×10^{-22} – 0.922×10^{-22} cm^3. The experimentally calculated polarizability value (1.007×10^{-22} cm^3) stretched out in the low frequency region and is well matched with the theoretically calculated value (1.009×10^{-22} cm^3) through Penn analysis. Further it is concluded that the electronic polarizability plays a major role in the polarization process.